



HAL
open science

Production of Single W Bosons in e^+e^- Interactions at $130 \leq \sqrt{s} \leq 183$ GeV and Limits on Anomalous $WW\gamma$ Couplings

M. Acciarri, O. Adriani, M. Aguilar-Benitez, S. Ahlen, J. Alcaraz, G. Alemani, J. Allaby, A. Aloisio, M G. Alviggi, G. Ambrosi, et al.

► To cite this version:

M. Acciarri, O. Adriani, M. Aguilar-Benitez, S. Ahlen, J. Alcaraz, et al.. Production of Single W Bosons in e^+e^- Interactions at $130 \leq \sqrt{s} \leq 183$ GeV and Limits on Anomalous $WW\gamma$ Couplings. Physics Letters B, 1998, 436, pp.417-427. in2p3-00023168

HAL Id: in2p3-00023168

<https://in2p3.hal.science/in2p3-00023168v1>

Submitted on 5 Nov 1998

HAL is a multi-disciplinary open access archive for the deposit and dissemination of scientific research documents, whether they are published or not. The documents may come from teaching and research institutions in France or abroad, or from public or private research centers.

L'archive ouverte pluridisciplinaire **HAL**, est destinée au dépôt et à la diffusion de documents scientifiques de niveau recherche, publiés ou non, émanant des établissements d'enseignement et de recherche français ou étrangers, des laboratoires publics ou privés.

**Production of Single W Bosons
in e^+e^- Interactions at $130 \leq \sqrt{s} \leq 183$ GeV
and Limits on Anomalous $WW\gamma$ Couplings**

L3 Collaboration

Abstract

We report on a study of single W boson production in a data sample collected by the L3 detector at centre-of-mass energies from 130 to 183 GeV. The signal consists of large missing energy final states with a single energetic lepton or two hadronic jets. The measured cross sections at five different centre-of-mass energies are consistent with the Standard Model expectations. The following limits on the anomalous $WW\gamma$ gauge couplings are derived at 95% CL: $-0.46 < \Delta\kappa_\gamma < 0.57$ and $-0.86 < \lambda_\gamma < 0.75$.

Submitted to *Phys.Lett. B*

1 Introduction

Precision measurements of the trilinear gauge boson couplings constitute critical tests of the Standard Model [1]. Extensive studies of the anomalous W couplings have been carried out in recent years by experiments at the Tevatron [2, 3] and at LEP [4, 5]. These studies focused so far on pair production of vector gauge bosons – WW, WZ and W γ .

The L3 experiment explored for the first time [6] another approach for studying the anomalous electromagnetic couplings of the W bosons by measuring the cross section of single W production ¹⁾

$$e^+e^- \rightarrow e^+\nu_e W^- \quad (1)$$

This process is a clean test of the WW γ vertex. The deviation of the gauge boson couplings from their Standard Model values is usually described in terms of five parameters: Δg_1^Z , $\Delta\kappa_Z$, $\Delta\kappa_\gamma$, λ_Z and λ_γ . The cross section of process (1) is shown in reference [7] to depend only on the parameters $\Delta\kappa_\gamma$ and λ_γ . Any non-zero value of these parameters, if observed, would indicate that W bosons have internal structure.

The cross section of process (1) is expected to be small at LEP2 energies – of the order 0.5 pb [7]. However, despite the low statistics, this process is a sensitive probe of new physics beyond the Standard Model. A specific feature of single W production is a final-state positron (electron) produced at very low polar angle and therefore not detected, whereas the associated neutrino may carry a considerable transverse momentum. Thus the signature of this process is large transverse missing energy and either a single energetic lepton, if the W boson decays into lepton and neutrino, or two hadronic jets in case of hadronic W decays. This process constitutes a background to searches for new physics beyond the Standard Model with missing energy signatures .

In this paper we present a study of the process $e^+e^- \rightarrow e^+\nu_e W^-$ at centre-of-mass energies $130 \text{ GeV} \leq \sqrt{s} \leq 183 \text{ GeV}$ using both leptonic and hadronic decays of W bosons.

2 Data and Monte Carlo Samples

The data were collected by the L3 detector [8] at LEP from 1995 to 1997. The integrated luminosities are 6.1 pb⁻¹, 6.0 pb⁻¹, 10.9 pb⁻¹, 10.2 pb⁻¹ and 55.3 pb⁻¹ at the centre-of-mass energies 130 GeV, 136 GeV, 161 GeV, 172 GeV and 183 GeV, respectively.

For the efficiency studies a sample of $e^+e^- \rightarrow e^+\nu_e f f'$ events was generated using the GRC4F [9] and EXCALIBUR [10] Monte Carlo generators. For the background studies the following Monte Carlo programs were used: KORALZ [11] ($e^+e^- \rightarrow \mu^+\mu^-(\gamma)$, $\tau^+\tau^-(\gamma)$), KORALW [12] ($e^+e^- \rightarrow W^+W^- \rightarrow f f' f f'$), BHAGENE3 [13] ($e^+e^- \rightarrow e^+e^-(\gamma)$), TEEGG [14] ($e^+e^- \rightarrow e^+e^-\gamma$), PYTHIA [15] ($e^+e^- \rightarrow q\bar{q}(\gamma)$, $e^+e^- \rightarrow ZZ$), PYTHIA and PHOJET [16] ($e^+e^- \rightarrow e^+e^-e^+e^-$, $e^+e^-\mu^+\mu^-$, $e^+e^-\tau^+\tau^-$, $e^+e^-q\bar{q}$), EXCALIBUR and GRC4F ($e^+e^- \rightarrow f f' f f'$).

The Monte Carlo events are simulated in the L3 detector using the GEANT 3.15 program [17], which takes into account the effects of energy loss, multiple scattering and showering in the detector. The GHEISHA program [18] is used to simulate hadronic interactions in the detector. The number of simulated background events for the most important background channels corresponds to at least 100 times the collected luminosity.

¹⁾The charge conjugate reactions are understood to be included throughout the paper.

3 Analysis Procedures

In the analysis described below, the signal is defined as $e^+e^- \rightarrow e^+\nu_e f f'$ events that satisfy the following phase space requirements [6]:

$$\begin{aligned} |\cos \theta_{e+}| &> 0.997 \\ \min(E_f, E_{f'}) &> 15 \text{ GeV} \\ |\cos \theta_{e-}| &< 0.75, \quad \text{for } e^+\nu_e e^-\bar{\nu}_e \text{ events only,} \end{aligned} \tag{2}$$

where θ_{e+} (θ_{e-}) is the polar angle of the outgoing positron (electron), and E_f and $E_{f'}$ are the fermion energies. The $e^+e^- \rightarrow e^+\nu_e f f'$ events that do not satisfy these conditions predominantly consist of W pair production.

Inside this region of phase space the single W production dominates since it peaks strongly at $|\cos \theta_{e+}| \sim 1$. On average it accounts for 90% of all events in this region, the remaining 10% being mostly non-resonant final states. The purity depends slightly on the centre-of-mass energy. For the $e^+\nu_e e^-\bar{\nu}_e$ final states the purity is lower than for other signal final states, it amounts to 75% on average.

There are two distinct signatures for the signal events: single leptons, $e^+\nu_e W^- \rightarrow e^+\nu_e \ell^- \bar{\nu}_\ell$, and acoplanar jet pairs, $e^+\nu_e W^- \rightarrow e^+\nu_e q q'$. Each analysis channel requires its own optimised selection criteria. For all leptonic channels cut-based analyses are used, similar to those described in our previous publication [6]. For the hadronic channel a neural network analysis is implemented. In the neural network analysis nine event variables are combined using a feed-forward neural network [19], with one hidden layer and one output node. The neural network output spectrum is used for the final differentiation between the signal and the background.

The background to process (1) is dominated by the four-fermion final states $\ell^- \bar{\nu}_\ell f f'$ from W -pair production. This contribution also depends on anomalous trilinear couplings. The use of the normalisation of this background as an additional constraint leads to an increase in the sensitivity of our data to anomalous couplings and allows to perform a simultaneous variation of both λ_γ and $\Delta\kappa_\gamma$ couplings in the fit.

3.1 Leptonic Final States

A distinct feature of the process $e^+e^- \rightarrow e^+\nu_e W^-$, $W^- \rightarrow \ell^- \bar{\nu}_\ell$ is a high-energy lepton from W decay with no other significant activity in the detector.

Events with one charged lepton (electron, muon or tau) with an energy of at least 15 GeV are selected. The lepton identification is based on the energy distribution in the electromagnetic and hadron calorimeters with respect to the trajectory of charged tracks. Events containing tracks that do not belong to the lepton are rejected. The visible energy, E_{vis} , is calculated as the sum of the lepton energy, E_ℓ , and the energies of all neutral clusters in the event. The ratio E_ℓ/E_{vis} for events preselected as described above is shown in Figure 1a for the single muon selection at 183 GeV. The requirement $E_\ell/E_{\text{vis}} > 0.92$ suppresses background from two-fermion production $e^+e^- \rightarrow \ell^+\ell^-(\gamma)$. In addition, the energy in the 0.44 rad azimuthal angle sector around the missing energy direction must be below 1 GeV. For the single electron final states, the polar angle is required to be $|\cos \theta_e| < 0.7$ and the electron energy must exceed 20 GeV. These additional requirements reduce the contribution from Bhabha and Compton scattering and from the process $e^+e^- \rightarrow e^+e^-\nu\bar{\nu}$ where the e^+e^- pair originates from a low-mass virtual photon.

The energy deposition in the forward calorimeters, E_{FB} , must be smaller than 60 GeV (Figure 1b) in order to suppress background from two-fermion processes, $e^+e^- \rightarrow \ell^+\ell^-(\gamma)$, and two-photon interactions, $e^+e^- \rightarrow e^+e^-ff'$. This criterion is significantly relaxed compared to our published analysis [6] as it was found that the sample purity does not depend on the cut value in the range from 15 GeV to 60 GeV. The final muon energy spectrum at 183 GeV is shown in Figure 1c together with the Monte Carlo expectations for the signal and background.

The number of observed events, the signal and background expectations at different centre-of-mass energies are presented in Table 1 for all the leptonic channels. There is good agreement between the data and the Standard Model expectations. The expected signal fraction in the selected single lepton samples is typically 50-70% at all centre-of-mass energies. The signal efficiency ranges from 25% for the tau channel to 65-70% for the electron and muon channels. The new selection criteria are used to analyse all the data. The candidates from the 161 GeV and 172 GeV data samples reported in our previous publication are still selected and the signal efficiencies and the background estimates are fully compatible with those reported in reference [6].

3.2 Hadronic Final States

The selection of candidates for the process $e^+e^- \rightarrow e^+\nu_e W^-$, $W^- \rightarrow qq'$ is based on the following requirements: two acoplanar hadronic jets, no leptons, and large missing transverse energy.

High multiplicity hadronic events with at least five charged tracks are selected with large energy deposition in the electromagnetic calorimeter, $E_{\text{ECAL}} > 10$ GeV, and large total visible energy, $E_{\text{vis}} > 60$ GeV. All energy clusters in the event are combined to form two hadronic jets using the DURHAM algorithm [20]. The invariant mass of the two jets must be in the range $40 \text{ GeV} < M_{\text{vis}} < 120 \text{ GeV}$. The energy in the forward luminosity calorimeters is required to be smaller than 60 GeV. These cuts reduce contributions from the purely leptonic final states $e^+e^- \rightarrow e^+e^-(\gamma)$, $\mu^+\mu^-(\gamma)$, $\tau^+\tau^-(\gamma)$ and two-photon interactions $e^+e^- \rightarrow e^+e^-q\bar{q}$ while keeping a significant fraction of hadronic events from $e^+e^- \rightarrow Z(\gamma)$, $e^+e^- \rightarrow W^+W^-$ and $e^+e^- \rightarrow ZZ$.

To reject events from the two-fermion production process $e^+e^- \rightarrow q\bar{q}(\gamma)$ the transverse missing energy is required to exceed 15 GeV. The missing momentum vector must point at least 0.30 rad away from the beam axis and the energy in the 0.44 rad azimuthal sector around its direction must be below 20 GeV. In addition, the opening angle between the two jets in the plane perpendicular to the beam direction must not exceed 3.0 rad.

Events containing identified leptons with energy greater than 20 GeV are rejected in order to suppress the remaining background from $e^+e^- \rightarrow W^+W^-$ where one of the W bosons decays into leptons. Three jets are formed for every remaining event using the DURHAM algorithm. The stereo angle, Ω , defined by the directions of these jets is required to be smaller than 5.5 rad. In addition, the distance scale parameter of the JADE algorithm [21] for which the number of jets in the event changes from two to three must not exceed 0.06, and the respective parameter for resolving three jets to four must be smaller than 0.015.

The number of observed events, the signal and background expectations at different centre-of-mass energies are presented in Table 1. The number of observed events is consistent with the Standard Model predictions. The signal efficiency ranges from 40% to 60% at low and high centre-of-mass energies, respectively. The expected signal fraction in the selected samples varies from 50% at $\sqrt{s} = 130 - 136$ GeV to 15% at $\sqrt{s} = 172 - 183$ GeV. This behaviour is

due to the fast rise of the WW cross section. The invariant mass distribution for the selected events at $\sqrt{s} = 183$ GeV is shown in Figure 2a.

To differentiate further between the signal and the WW background, the discriminant variable NN_{out} is constructed using a neural network approach. The inputs to the neural network include event shape variables, the event invariant mass, the masses of the two jets, the total missing momentum and the stereo angle Ω . The use of the neural network permits to increase the signal fraction in the selected samples at $\sqrt{s} = 172 - 183$ GeV to approximately 60% for large neural network output values, as demonstrated in Figure 2b. The neural network results at $\sqrt{s} = 161 - 172$ GeV are consistent with our previous publication [6]. They improve and supersede the previous results. At $\sqrt{s} = 130 - 136$ GeV the contribution of WW background is small. Therefore, at these energies a cut-based approach is used similar to the one from our previous publication [6].

As a cross-check of neural network performance a fit of the WW cross section is performed at $\sqrt{s} = 183$ GeV, fixing the single W contribution to the Monte Carlo prediction. The fit result is $\sigma_{\text{WW}} = 15.9_{-2.2}^{+2.4}$ pb, in good agreement with the Standard Model expectation.

4 Systematic Errors

The dominant systematic error of the present analysis arises from the uncertainty in the signal modelling. It is found to be 5-10% comparing the signal efficiencies estimated using the two Monte Carlo generators, GRC4F and EXCALIBUR. This discrepancy is treated as a systematic error fully correlated between all the selection channels.

The systematic error on the expected number of background events is essentially due to the limited Monte Carlo statistics, with smaller contributions from the uncertainties on the cross sections and the selection efficiency for the background processes. The overall error on the number of background events in the individual channels varies from 5-6% at $\sqrt{s} = 183$ GeV to 30-60% at $\sqrt{s} = 130$ GeV, where the number of expected events in the single lepton channels is of the order 0.1. However, these uncertainties are uncorrelated among individual channels and different centre-of-mass energies and therefore have negligible impact on the final results.

5 Results

The total cross section of all signal processes is determined from a binned maximum-likelihood fit to the energy spectra of leptons and the neural network output distributions for hadrons. Examples of these distributions are presented in Figures 1c and 2b. The background shapes and normalisations are fixed to the Monte Carlo predictions. The measured signal cross section, $\sigma(e^+e^- \rightarrow e\nu_e W)$, corresponds to that of the process $e^+e^- \rightarrow e\nu_e f f'$, where $f f'$ denotes a sum of $\ell\nu_\ell$ and $q q'$ final states satisfying the phase space conditions (2). The energy dependence of $\sigma(e^+e^- \rightarrow e\nu_e W)$ is assumed to be as predicted by GRC4F, and the only free parameter in the fit is the cross section at $\sqrt{s} = 183$ GeV. It is found to be

$$\sigma(e^+e^- \rightarrow e\nu_e W) = 0.62_{-0.18}^{+0.19} (\text{stat.}) \pm 0.04 (\text{syst.}) \text{ pb} \quad (3)$$

in agreement with the Standard Model expectation of 0.50 pb as obtained with GRC4F. The existence of single W production is established at a confidence level that exceeds 99.9%.

Cross sections at each centre-of-mass energy are determined from similar fits that use only the corresponding data samples. The cross section dependence on the centre-of-mass energy agrees well with the Standard Model predictions as shown in Figure 3 and Table 2.

Limits on the anomalous electromagnetic couplings, $\Delta\kappa_\gamma$ and λ_γ , are determined from a binned maximum-likelihood fit similar to the one used for the cross section determination. In the fit each Monte Carlo event is assigned a weight that depends on the event kinematics and anomalous couplings. The dependence of the background processes on the anomalous couplings is also taken into account. The weight is calculated using the EXCALIBUR matrix element with additional constraints on the anomalous couplings Δg_1^Z , $\Delta\kappa_Z$ and λ_Z arising from the $SU(2) \times U(1)$ gauge invariance: $\Delta\kappa_Z = \Delta g_1^Z - \tan^2 \theta_w \cdot \Delta\kappa_\gamma$ and $\lambda_Z = \lambda_\gamma$. These constraints affect only the background contributions, as the signal process depends on λ_γ and $\Delta\kappa_\gamma$ only. The general analysis of Δg_1^Z , λ_γ and $\Delta\kappa_\gamma$ can only be done with full consideration of the W-pair production. In the present analysis we assume that the anomalous weak charge of the W bosons is zero, $\Delta g_1^Z = 0$, and focus on the electromagnetic properties of W bosons.

The dominant systematic error arises from the difference in the signal efficiency estimated using the two Monte Carlo generators, GRC4F and EXCALIBUR. This uncertainty is found to be 5-10% depending on the centre-of-mass energy. It is assumed to be Gaussian and fully correlated between individual selection channels. The likelihood function is convoluted with this Gaussian in the fit.

Both λ_γ and $\Delta\kappa_\gamma$ are varied freely in the fit that yields $\Delta\kappa_\gamma = 0.06_{-0.26}^{+0.27}$ and $\lambda_\gamma = -0.48_{-0.21}^{+0.44}$, consistent with the absence of anomalous contribution to $WW\gamma$ couplings²⁾. The correlation between these two parameters in the fit is found to be 0.26. The behaviour of the log-likelihood function in the vicinity of its minimum is presented in Figure 4. For comparison, the individual contributions to the log-likelihood function from the signal and the background events are also calculated by fixing one of the two expectations to the corresponding Standard Model prediction (Figure 4). It follows from this comparison that most of the sensitivity of the present analysis to $\Delta\kappa_\gamma$ is due to process (1), whereas the sensitivity to λ_γ is shared approximately equally between the single W and the W pair production.

The limits on the deviations of these couplings from the Standard Model values are set at 95% confidence level to:

$$\begin{aligned} -0.46 &< \Delta\kappa_\gamma < 0.57 \\ -0.86 &< \lambda_\gamma < 0.75 \end{aligned} \tag{4}$$

These limits represent a considerable improvement in the sensitivity to the anomalous couplings λ_γ and $\Delta\kappa_\gamma$ compared to our previous publications [4, 6]. The 68% and 95% confidence level contours are presented in Figure 5. These limits are among the most stringent presently available [2–5].

Acknowledgements

We wish to express our gratitude to the CERN accelerator divisions for the excellent performance of the LEP machine. We acknowledge the efforts of all engineers and technicians who have participated in the construction and maintenance of this experiment.

²⁾Another set of constraints, that assumes no anomalous contribution to the weak interactions of the W bosons – $\Delta g_Z = \Delta\kappa_Z = \lambda_Z = 0$, was also studied. The results of this study are almost identical to those reported in this paper.

References

- [1] S.L.Glashow, Nucl.Phys. **22** (1961) 579;
S.Weinberg, Phys.Rev.Lett. **19** (1967) 1264;
A.Salam, "Elementary Particle Theory", Ed. N.Svartholm, Stockholm, "Almqvist and Wiksell", (1968), 367.
- [2] F.Abe *et al.*, CDF Collaboration, Phys.Rev.Lett. **74** (1995) 1936; Phys.Rev.Lett. **75** (1995) 1017; Phys.Rev.Lett. **78** (1997) 4536.
- [3] S.Abachi *et al.*, D0 Collaboration, Phys.Rev.Lett. **79** (1997) 1441; Phys.Rev. **D56** (1997) 6742.
- [4] M.Acciarri *et al.*, L3 Collaboration, Phys.Lett. **B413** (1997) 176.
- [5] P.Abreu *et al.*, DELPHI Collaboration, Phys.Lett. **B397** (1997) 158;
K.Ackerstaff *et al.*, OPAL Collaboration, Phys.Lett. **B397** (1997) 147;
K.Ackerstaff *et al.*, OPAL Collaboration, CERN-PPE-97-125, Subm. to Z. Phys. C;
R. Barate *et al.*, ALEPH Collaboration, CERN-PPE-97-166, Subm. to Phys.Lett. B.
- [6] M.Acciarri *et al.*, L3 Collaboration, Phys. Lett. **B403** (1997) 168.
- [7] T.Tsukamoto and Y.Kurihara, Phys.Lett. **B389** (1996), 162.
- [8] B.Adeva *et al.*, L3 Collaboration, Nucl.Instr.Meth. **A289** (1990) 35; J.A.Bakken *et al.*, Nucl.Instr.Meth. **A275** (1989) 81; O.Adriani *et al.*, Nucl.Instr.Meth. **A302** (1991) 53; B.Adeva *et al.*, Nucl.Instr.Meth. **A323** (1992) 109; K.Deiters *et al.*, Nucl.Instr.Meth. **A323** (1992) 162; M.Chemarin *et al.*, Nucl.Instr.Meth. **A349** (1994) 345; M.Acciarri *et al.*, Nucl.Instr.Meth. **A351** (1994) 300; G.Basti *et al.*, Nucl.Instr.Meth. **A374** (1996) 293; A.Adam *et al.*, Nucl.Instr.Meth. **A383** (1996) 342.
- [9] J.Fujimoto *et al.*, Comp.Phys.Comm. **100** (1997) 128.
- [10] F.A.Berends, R.Pittau and R.Kleiss, Comp.Phys.Comm. **85** (1995) 437.
- [11] S.Jadach, B.F.L.Ward and Z.Wąs, Comp.Phys.Comm. **79** (1994) 503.
- [12] M.Skrzypek *et al.*, Comp.Phys.Comm. **94** (1996) 216; Phys.Lett. **B372** (1996) 289.
- [13] J.H.Field, Phys.Lett. **B323** (1994) 432; J.H.Field and T. Riemann, Comp.Phys.Comm. **94** (1996) 53.
- [14] D.Karlen, Nucl.Phys. **B289** (1987) 23.
- [15] T.Sjöstrand, CERN-TH/7112/93 (1993), revised August 1995; Comp.Phys.Comm. **82** (1994) 74.
- [16] R.Engel, Z.Phys. **C66** (1995) 203; R.Engel, J.Ranft and S.Roesler, Phys.Rev. **D52** (1995) 1459.
- [17] R.Brun *et al.*, preprint CERN DD/EE/84-1 (Revised 1987).
- [18] H.Fesefeldt, RWTH Aachen Report PITHA 85/02 (1985).

- [19] L.Lönnblad, C. Peterson and T.Rögnvaldsson, Nucl.Phys. **B349** (1991) 675;
C.Peterson *et al.*, Comp.Phys.Comm. **81** (1994) 185.
- [20] S.Catani *et al.*, Phys.Lett. **B269** (1991) 432;
S.Bethke *et al.*, Nucl.Phys. **B370** (1992) 310.
- [21] JADE Collaboration, W. Bartel *et al.*, Z. Phys. **C33** (1986) 23; S. Bethke *et al.*, Phys.
Lett. **B213** (1988) 235.

The L3 Collaboration:

M. Acciarri,²⁸ O. Adriani,¹⁷ M. Aguilar-Benitez,²⁷ S. Ahlen,¹² J. Alcaraz,²⁷ G. Alemani,²³ J. Allaby,¹⁸ A. Aloisio,³⁰ M.G. Alvigi,³⁰ G. Ambrosi,²⁰ H. Anderhub,⁴⁹ V.P. Andreev,^{7,38} T. Angelescu,¹⁴ F. Anselmo,¹⁰ A. Arefiev,²⁹ T. Azemoon,³ T. Aziz,¹¹ P. Bagnaia,³⁷ L. Baksay,⁴⁴ S. Banerjee,¹¹ Sw. Banerjee,¹¹ K. Banicz,⁴⁶ A. Barczyk,^{49,47} R. Barillere,¹⁸ L. Barone,³⁷ P. Bartalini,²³ A. Baschirotto,²⁸ M. Basile,¹⁰ R. Battiston,³⁴ A. Bay,²³ F. Becattini,¹⁷ U. Becker,¹⁶ F. Behner,⁴⁹ J. Berdugo,²⁷ P. Berges,¹⁶ B. Bertucci,³⁴ B.L. Betev,⁴⁹ S. Bhattacharya,¹¹ M. Biasini,³⁴ A. Biland,⁴⁹ G.M. Bilei,³⁴ J.J. Blaising,⁴ S.C. Blyth,³⁵ G.J. Bobbink,² R. Bock,¹ A. Böhm,¹ L. Boldizar,¹⁵ B. Borgia,^{18,37} D. Bourilkov,⁴⁹ M. Bourquin,²⁰ S. Braccini,²⁰ J.G. Branson,⁴⁰ V. Brigljevic,⁴⁹ I.C. Brock,³⁵ A. Buffini,¹⁷ A. Buijs,⁴⁵ J.D. Burger,¹⁶ W.J. Burger,³⁴ J. Busenitz,⁴⁴ A. Button,³ X.D. Cai,¹⁶ M. Campanelli,⁴⁹ M. Capell,¹⁶ G. Cara Romeo,¹⁰ G. Carlino,³⁰ A.M. Cartacci,¹⁷ J. Casaus,²⁷ G. Castellini,¹⁷ F. Cavallari,³⁷ N. Cavallo,³⁰ C. Cecchi,²⁰ M. Cerrada,²⁷ F. Cesaroni,²⁴ M. Chamizo,²⁷ Y.H. Chang,⁵¹ U.K. Chaturvedi,¹⁹ M. Chemarin,²⁶ A. Chen,⁵¹ G. Chen,⁸ G.M. Chen,⁸ H.F. Chen,²¹ H.S. Chen,⁸ X. Chereau,⁴ G. Chiefari,³⁰ C.Y. Chien,⁵ L. Cifarelli,³⁹ F. Cindolo,¹⁰ C. Civinini,¹⁷ I. Clare,¹⁶ R. Clare,¹⁶ G. Coignet,⁴ A.P. Colijn,² N. Colino,²⁷ S. Costantini,⁹ F. Cotoroba,¹⁴ B. de la Cruz,²⁷ A. Csilling,¹⁵ T.S. Dai,¹⁶ R.D' Alessandro,¹⁷ R. de Asmundis,³⁰ A. Degré,⁴ K. Deiters,⁴⁷ D. della Volpe,³⁰ P. Denes,³⁶ F. DeNotaristefani,³⁷ M. Diemoz,³⁷ D. van Dierendonck,² F. Di Lodovico,⁴⁹ C. Dionisi,^{18,37} M. Dittmar,⁴⁹ A. Dominguez,⁴⁰ A. Doria,³⁰ M.T. Dova,^{9,‡} D. Duchesneau,⁴ P. Duinker,² I. Duran,⁴¹ S. Easo,³⁴ H. El Mamouni,²⁶ A. Engler,³⁵ F.J. Eppling,¹⁶ F.C. Erne,² J.P. Ernenwein,²⁶ P. Extermann,²⁰ M. Fabre,⁴⁷ R. Faccini,³⁷ M.A. Falagan,²⁷ S. Falciiano,³⁷ A. Favara,¹⁷ J. Fay,²⁶ O. Fedin,³⁸ M. Felcini,⁴⁹ T. Ferguson,³⁵ F. Ferroni,³⁷ H. Fesefeldt,¹ E. Fiandrini,³⁴ J.H. Field,²⁰ F. Filthaut,¹⁸ P.H. Fisher,¹⁶ I. Fisk,⁴⁰ G. Forconi,¹⁶ L. Fredj,²⁰ K. Freudenreich,⁴⁹ C. Furetta,²⁸ Yu. Galaktionov,^{29,16} S.N. Ganguli,¹¹ P. Garcia-Abia,⁶ M. Gataullin,³³ S.S. Gau,¹³ S. Gentile,³⁷ N. Gheordanescu,¹⁴ S. Giagu,³⁷ S. Goldfarb,²³ J. Goldstein,¹² Z.F. Gong,²¹ A. Gougas,⁵ G. Gratta,³³ M.W. Gruenewald,⁹ R. van Gulik,² V.K. Gupta,³⁶ A. Gurtu,¹¹ L.J. Gutay,⁴⁶ D. Haas,⁶ B. Hartmann,¹ A. Hasan,³¹ D. Hatzifotiadou,¹⁰ T. Hebbeker,⁹ A. Hervé,¹⁸ P. Hidas,¹⁵ J. Hirschfelder,³⁵ W.C. van Hoek,³² H. Hofer,⁴⁹ H. Hoorani,³⁵ S.R. Hou,⁵¹ G. Hu,⁵ I. Iashvili,⁴⁸ B.N. Jin,⁸ L.W. Jones,³ P. de Jong,¹⁸ L. Josa-Mutuberria,²⁷ R.A. Khan,¹⁹ D. Kamrad,⁴⁸ J.S. Kapustinsky,²⁵ M. Kaur,^{19,‡} M.N. Kienzle-Focacci,²⁰ D. Kim,³⁷ D.H. Kim,⁴³ J.K. Kim,⁴³ S.C. Kim,⁴³ W.W. Kinnison,²⁵ A. Kirkby,³³ D. Kirkby,³³ J. Kirkby,¹⁸ D. Kiss,¹⁵ W. Kittel,³² A. Klimentov,^{16,29} A.C. König,³² A. Kopp,⁴⁸ I. Korolko,²⁹ V. Koutsenko,^{16,29} R.W. Kraemer,³⁵ W. Krenz,¹ A. Kunin,^{16,29} P. Lacentre,^{48,‡,‡} P. Ladron de Guevara,²⁷ I. Laktineh,²⁶ G. Landi,¹⁷ C. Lapoint,¹⁶ K. Lassila-Perini,⁴⁹ P. Laurikainen,²² A. Lavorato,³⁹ M. Lebeau,¹⁸ A. Lebedev,¹⁶ P. Lebrun,²⁶ P. Lecomte,⁴⁹ P. Lecoq,¹⁸ P. Le Coultre,⁴⁹ H.J. Lee,⁹ J.M. Le Goff,¹⁸ R. Leiste,⁴⁸ E. Leonardi,³⁷ P. Levchenko,³⁸ C. Li,²¹ C.H. Lin,⁵¹ W.T. Lin,⁵¹ F.L. Linde,^{2,18} L. Lista,³⁰ Z.A. Liu,⁸ W. Lohmann,⁴⁸ E. Longo,³⁷ W. Lu,³³ Y.S. Lu,⁸ K. Lübelmeyer,¹ C. Luci,^{18,37} D. Luckey,¹⁶ L. Luminari,³⁷ W. Lustermann,⁴⁹ W.G. Ma,²¹ M. Maity,¹¹ G. Majumder,¹¹ L. Malgeri,¹⁸ A. Malinin,²⁹ C. Mañá,²⁷ D. Mangeol,³² P. Marchesini,⁴⁹ G. Mariani,^{44,¶} A. Marin,¹² J.P. Martin,²⁶ F. Marzano,³⁷ G.G.G. Massaro,² K. Mazumdar,¹¹ R.R. McNeil,⁷ S. Mele,¹⁸ L. Merola,³⁰ M. Meschini,¹⁷ W.J. Metzger,³² M. von der Mey,¹ D. Migani,¹⁰ A. Mihul,¹⁴ A.J.W. van Mil,³² H. Milcent,¹⁸ G. Mirabelli,³⁷ J.Mnich,¹⁸ P. Molnar,⁹ B. Monteoloni,¹⁷ R. Moore,³ T. Moulík,¹¹ R. Mount,³³ F. Muheim,²⁰ A.J.M. Muijs,² S. Nahn,¹⁶ M. Napolitano,³⁰ F. Nessi-Tedaldi,⁴⁹ H. Newman,³³ T. Niessen,¹ A. Nippe,²³ A. Nisati,³⁷ H. Nowak,⁴⁸ Y.D. Oh,⁴³ G. Organtini,³⁷ R. Ostonen,²² S. Palit,¹³ C. Palomares,²⁷ D. Pandoulas,¹ S. Paoletti,³⁷ P. Paolucci,³⁰ H.K. Park,³⁵ I.H. Park,⁴³ G. Pascale,³⁷ G. Passaleva,¹⁸ S. Patricelli,³⁰ T. Paul,¹³ M. Pauluzzi,³⁴ C. Paus,¹⁸ F. Pauss,⁴⁹ D. Peach,¹⁸ Y.J. Pei,¹ S. Pensotti,²⁸ D. Perret-Gallix,⁴ B. Petersen,³² S. Petrak,⁹ A. Pevsner,⁵ D. Piccolo,³⁰ M. Pieri,¹⁷ P.A. Piroué,³⁶ E. Pistolesi,²⁸ V. Plyaskin,²⁹ M. Pohl,⁴⁹ V. Pojidaev,^{29,17} H. Postema,¹⁶ J. Potier,¹⁸ N. Produit,²⁰ D. Prokofiev,³⁸ J. Quartieri,³⁹ G. Rahal-Callot,⁴⁹ N. Raja,¹¹ P.G. Rancoita,²⁸ M. Rattaggi,²⁸ G. Raven,⁴⁰ P. Razis,³¹ D. Ren,⁴⁹ M. Rescigno,³⁷ S. Reucroft,¹³ T. van Rhee,⁴⁵ S. Riemann,⁴⁸ K. Riles,³ A. Robohm,⁴⁹ J. Rodin,⁴⁴ B.P. Roe,³ L. Romero,²⁷ S. Rosier-Lees,⁴ S. Roth,¹ J.A. Rubio,¹⁸ D. Ruschmeier,⁹ H. Rykaczewski,⁴⁹ J. Salicio,¹⁸ E. Sanchez,²⁷ M.P. Sanders,³² M.E. Sarakinos,²² C. Schäfer,¹ V. Schegelsky,³⁸ S. Schmidt-Kaerst,¹ D. Schmitz,¹ N. Scholz,⁴⁹ H. Schopper,⁵⁰ D.J. Schotanus,³² J. Schwenke,¹ G. Schwering,¹ C. Sciacca,³⁰ D. Sciarrino,²⁰ L. Servoli,³⁴ S. Shevchenko,³³ N. Shivarov,⁴² V. Shoutko,²⁹ J. Shukla,²⁵ E. Shumilov,²⁹ A. Shvorob,³³ T. Siedenbarg,¹ D. Son,⁴³ B. Smith,¹⁶ P. Spillantini,¹⁷ M. Steuer,¹⁶ D.P. Stickland,³⁶ A. Stone,⁷ H. Stone,³⁶ B. Stoyanov,⁴² A. Straessner,¹ K. Sudhakar,¹¹ G. Sultanov,¹⁹ L.Z. Sun,²¹ G.F. Susinno,²⁰ H. Suter,⁴⁹ J.D. Swain,¹⁹ X.W. Tang,⁸ L. Tauscher,⁶ L. Taylor,¹³ C. Timmermans,³² Samuel C.C. Ting,¹⁶ S.M. Ting,¹⁶ S.C. Tonwar,¹¹ J. Tóth,¹⁵ C. Tully,³⁶ K.L. Tung,⁸ Y. Uchida,¹⁶ J. Ulbricht,⁴⁹ E. Valente,³⁷ G. Vesztegombi,¹⁵ I. Vetlitsky,²⁹ G. Viertel,⁴⁹ M. Vivargent,⁴ S. Vlachos,⁶ H. Vogel,³⁵ H. Vogt,⁴⁸ I. Vorobiev,^{18,29} A.A. Vorobyov,³⁸ A. Vorvolakos,³¹ M. Wadhwa,⁷ W. Wallraff,¹ J.C. Wang,¹⁶ X.L. Wang,²¹ Z.M. Wang,²¹ A. Weber,¹ S.X. Wu,¹⁶ S. Wynhoff,¹ J. Xu,¹² Z.Z. Xu,²¹ B.Z. Yang,²¹ C.G. Yang,⁸ H.J. Yang,⁸ M. Yang,⁸ J.B. Ye,²¹ S.C. Yeh,⁵² J.M. You,³⁵ An. Zalite,³⁸ Yu. Zalite,³⁸ P. Zemp,⁴⁹ Y. Zeng,¹ Z.P. Zhang,²¹ B. Zhou,¹² G.Y. Zhu,⁸ R.Y. Zhu,³³ A. Zichichi,^{10,18,19} F. Ziegler,⁴⁸ G. Zilizi,^{44,¶}

- 1 I. Physikalisches Institut, RWTH, D-52056 Aachen, FRG[§]
 - III. Physikalisches Institut, RWTH, D-52056 Aachen, FRG[§]
 - 2 National Institute for High Energy Physics, NIKHEF, and University of Amsterdam, NL-1009 DB Amsterdam, The Netherlands
 - 3 University of Michigan, Ann Arbor, MI 48109, USA
 - 4 Laboratoire d'Annecy-le-Vieux de Physique des Particules, LAPP, IN2P3-CNRS, BP 110, F-74941 Annecy-le-Vieux CEDEX, France
 - 5 Johns Hopkins University, Baltimore, MD 21218, USA
 - 6 Institute of Physics, University of Basel, CH-4056 Basel, Switzerland
 - 7 Louisiana State University, Baton Rouge, LA 70803, USA
 - 8 Institute of High Energy Physics, IHEP, 100039 Beijing, China[△]
 - 9 Humboldt University, D-10099 Berlin, FRG[§]
 - 10 University of Bologna and INFN-Sezione di Bologna, I-40126 Bologna, Italy
 - 11 Tata Institute of Fundamental Research, Bombay 400 005, India
 - 12 Boston University, Boston, MA 02215, USA
 - 13 Northeastern University, Boston, MA 02115, USA
 - 14 Institute of Atomic Physics and University of Bucharest, R-76900 Bucharest, Romania
 - 15 Central Research Institute for Physics of the Hungarian Academy of Sciences, H-1525 Budapest 114, Hungary[‡]
 - 16 Massachusetts Institute of Technology, Cambridge, MA 02139, USA
 - 17 INFN Sezione di Firenze and University of Florence, I-50125 Florence, Italy
 - 18 European Laboratory for Particle Physics, CERN, CH-1211 Geneva 23, Switzerland
 - 19 World Laboratory, FBLJA Project, CH-1211 Geneva 23, Switzerland
 - 20 University of Geneva, CH-1211 Geneva 4, Switzerland
 - 21 Chinese University of Science and Technology, USTC, Hefei, Anhui 230 029, China[△]
 - 22 SEFT, Research Institute for High Energy Physics, P.O. Box 9, SF-00014 Helsinki, Finland
 - 23 University of Lausanne, CH-1015 Lausanne, Switzerland
 - 24 INFN-Sezione di Lecce and Università Degli Studi di Lecce, I-73100 Lecce, Italy
 - 25 Los Alamos National Laboratory, Los Alamos, NM 87544, USA
 - 26 Institut de Physique Nucléaire de Lyon, IN2P3-CNRS, Université Claude Bernard, F-69622 Villeurbanne, France
 - 27 Centro de Investigaciones Energeticas, Medioambientales y Tecnológicas, CIEMAT, E-28040 Madrid, Spain[‡]
 - 28 INFN-Sezione di Milano, I-20133 Milan, Italy
 - 29 Institute of Theoretical and Experimental Physics, ITEP, Moscow, Russia
 - 30 INFN-Sezione di Napoli and University of Naples, I-80125 Naples, Italy
 - 31 Department of Natural Sciences, University of Cyprus, Nicosia, Cyprus
 - 32 University of Nijmegen and NIKHEF, NL-6525 ED Nijmegen, The Netherlands
 - 33 California Institute of Technology, Pasadena, CA 91125, USA
 - 34 INFN-Sezione di Perugia and Università Degli Studi di Perugia, I-06100 Perugia, Italy
 - 35 Carnegie Mellon University, Pittsburgh, PA 15213, USA
 - 36 Princeton University, Princeton, NJ 08544, USA
 - 37 INFN-Sezione di Roma and University of Rome, "La Sapienza", I-00185 Rome, Italy
 - 38 Nuclear Physics Institute, St. Petersburg, Russia
 - 39 University and INFN, Salerno, I-84100 Salerno, Italy
 - 40 University of California, San Diego, CA 92093, USA
 - 41 Dept. de Física de Partículas Elementales, Univ. de Santiago, E-15706 Santiago de Compostela, Spain
 - 42 Bulgarian Academy of Sciences, Central Lab. of Mechatronics and Instrumentation, BU-1113 Sofia, Bulgaria
 - 43 Center for High Energy Physics, Adv. Inst. of Sciences and Technology, 305-701 Taejeon, Republic of Korea
 - 44 University of Alabama, Tuscaloosa, AL 35486, USA
 - 45 Utrecht University and NIKHEF, NL-3584 CB Utrecht, The Netherlands
 - 46 Purdue University, West Lafayette, IN 47907, USA
 - 47 Paul Scherrer Institut, PSI, CH-5232 Villigen, Switzerland
 - 48 DESY-Institut für Hochenergiephysik, D-15738 Zeuthen, FRG
 - 49 Eidgenössische Technische Hochschule, ETH Zürich, CH-8093 Zürich, Switzerland
 - 50 University of Hamburg, D-22761 Hamburg, FRG
 - 51 National Central University, Chung-Li, Taiwan, China
 - 52 Department of Physics, National Tsing Hua University, Taiwan, China
- [§] Supported by the German Bundesministerium für Bildung, Wissenschaft, Forschung und Technologie
[‡] Supported by the Hungarian OTKA fund under contract numbers T019181, F023259 and T024011.
[¶] Also supported by the Hungarian OTKA fund under contract numbers T22238 and T026178.
[‡] Supported also by the Comisión Interministerial de Ciencia y Tecnología.
[‡] Also supported by CONICET and Universidad Nacional de La Plata, CC 67, 1900 La Plata, Argentina.
[‡] Supported by Deutscher Akademischer Austauschdienst.
[◇] Also supported by Panjab University, Chandigarh-160014, India.
[△] Supported by the National Natural Science Foundation of China.

Table 1: The number of expected events from signal and background and the number of selected data events at different centre-of-mass energies. The background expectations are split into two categories: processes that do not depend on the anomalous couplings (Background 1) and those that do (Background 2).

Final state	Background 1	Background 2	Signal	Total expected	Data
$\sqrt{s} = 130 \text{ GeV}, \mathcal{L}_{\text{int}} = 6.1\text{pb}^{-1}$					
$e^+\nu_e e^-\bar{\nu}_e$	0.02	0.01	0.03	0.06	0
$e^+\nu_e\mu^-\bar{\nu}_\mu$	0.03	0.01	0.05	0.09	0
$e^+\nu_e\tau^-\bar{\nu}_\tau$	0.03	0.01	0.02	0.05	0
$e^+\nu_e q q'$	0.07	0.03	0.12	0.22	0
$\sqrt{s} = 136 \text{ GeV}, \mathcal{L}_{\text{int}} = 6.0\text{pb}^{-1}$					
$e^+\nu_e e^-\bar{\nu}_e$	0.05	0.01	0.06	0.11	0
$e^+\nu_e\mu^-\bar{\nu}_\mu$	0.03	0.01	0.06	0.10	0
$e^+\nu_e\tau^-\bar{\nu}_\tau$	0.03	0.01	0.02	0.06	0
$e^+\nu_e q q'$	0.21	0.07	0.24	0.51	1
$\sqrt{s} = 161 \text{ GeV}, \mathcal{L}_{\text{int}} = 10.9\text{pb}^{-1}$					
$e^+\nu_e e^-\bar{\nu}_e$	0.19	0.03	0.22	0.45	1
$e^+\nu_e\mu^-\bar{\nu}_\mu$	0.05	0.03	0.21	0.29	0
$e^+\nu_e\tau^-\bar{\nu}_\tau$	0.04	0.01	0.07	0.12	0
$e^+\nu_e q q'$	3.65	1.88	1.10	6.63	7
$\sqrt{s} = 172 \text{ GeV}, \mathcal{L}_{\text{int}} = 10.2\text{pb}^{-1}$					
$e^+\nu_e e^-\bar{\nu}_e$	0.20	0.06	0.32	0.58	0
$e^+\nu_e\mu^-\bar{\nu}_\mu$	0.05	0.05	0.26	0.36	0
$e^+\nu_e\tau^-\bar{\nu}_\tau$	0.03	0.03	0.10	0.16	1
$e^+\nu_e q q'$	1.42	8.68	1.50	11.60	15
$\sqrt{s} = 183 \text{ GeV}, \mathcal{L}_{\text{int}} = 55.3\text{pb}^{-1}$					
$e^+\nu_e e^-\bar{\nu}_e$	1.49	0.55	2.05	4.09	5
$e^+\nu_e\mu^-\bar{\nu}_\mu$	0.31	0.41	1.92	2.65	3
$e^+\nu_e\tau^-\bar{\nu}_\tau$	0.19	0.16	0.65	1.00	2
$e^+\nu_e q q'$	6.58	65.98	11.76	84.32	86

Table 2: The measured cross section values at different centre-of-mass energies together with their statistical and systematic errors. The absence of the negative-side statistical error at 130 GeV and 136 GeV indicate that zero signal cross section is not excluded at 68% confidence level.

\sqrt{s} (GeV)	$\sigma_{e^+\nu_e W^-}$ (pb)	$\Delta\sigma_{\text{stat}}^{\text{pos}}$ (pb)	$\Delta\sigma_{\text{stat}}^{\text{neg}}$ (pb)	$\Delta\sigma_{\text{syst}}$ (pb)
130	0.00	+0.22	—	0.02
136	0.21	+0.50	—	0.02
161	0.46	+0.47	-0.35	0.04
172	0.60	+0.59	-0.44	0.04
183	0.62	+0.22	-0.19	0.04

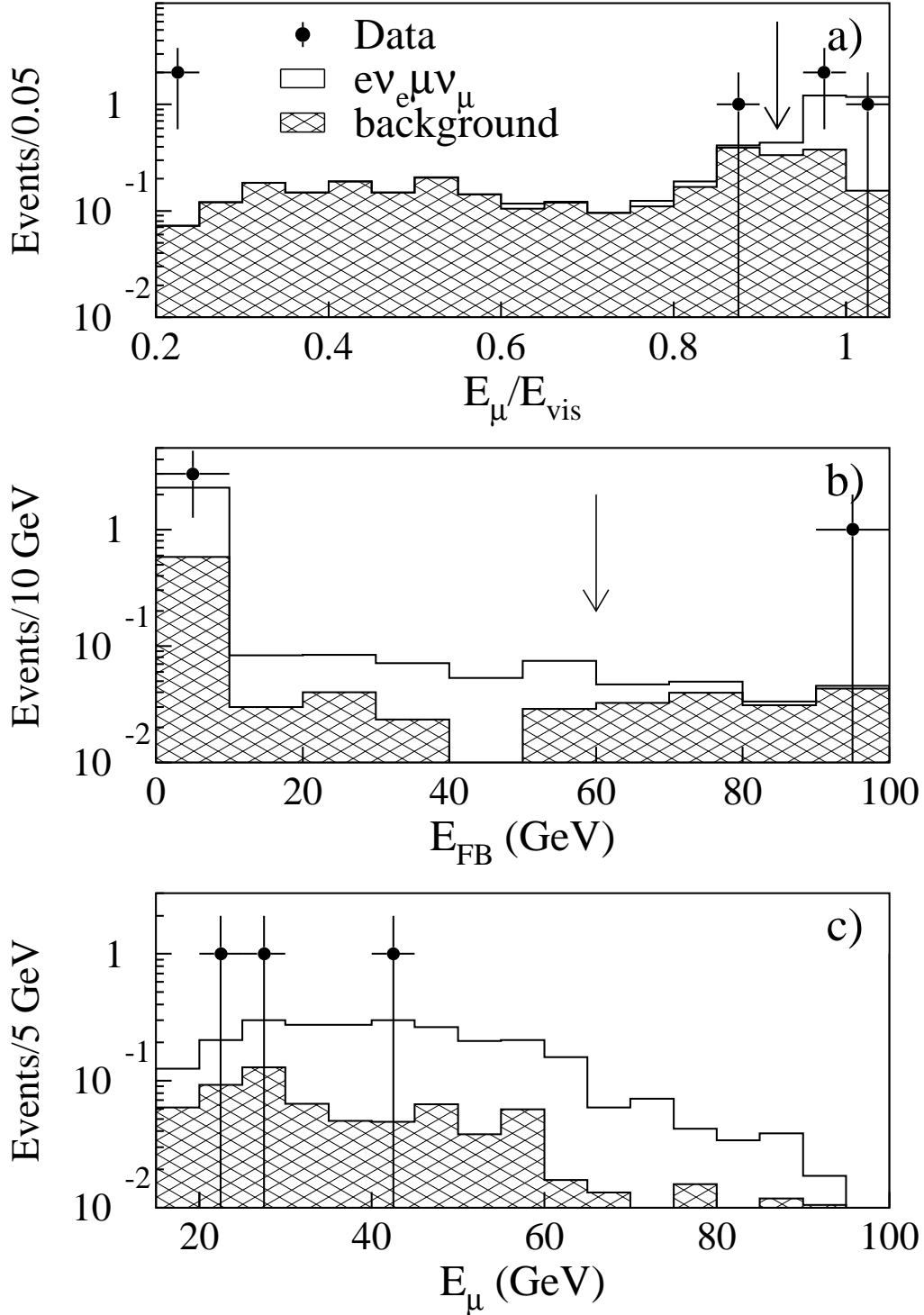


Figure 1: The distributions of the preselected single muon candidates at $\sqrt{s} = 183$ GeV: (a) the ratio E_μ/E_{vis} , (b) the energy depositions in the forward-backward luminosity calorimeters and (c) the muon energy spectrum. The dots are data, the open areas correspond to the contribution of $e^+\nu_e\mu^-\bar{\nu}_\mu$ final states and the hatched histograms represent the background. The arrows in (a) and (b) indicate the corresponding values of the applied cuts.

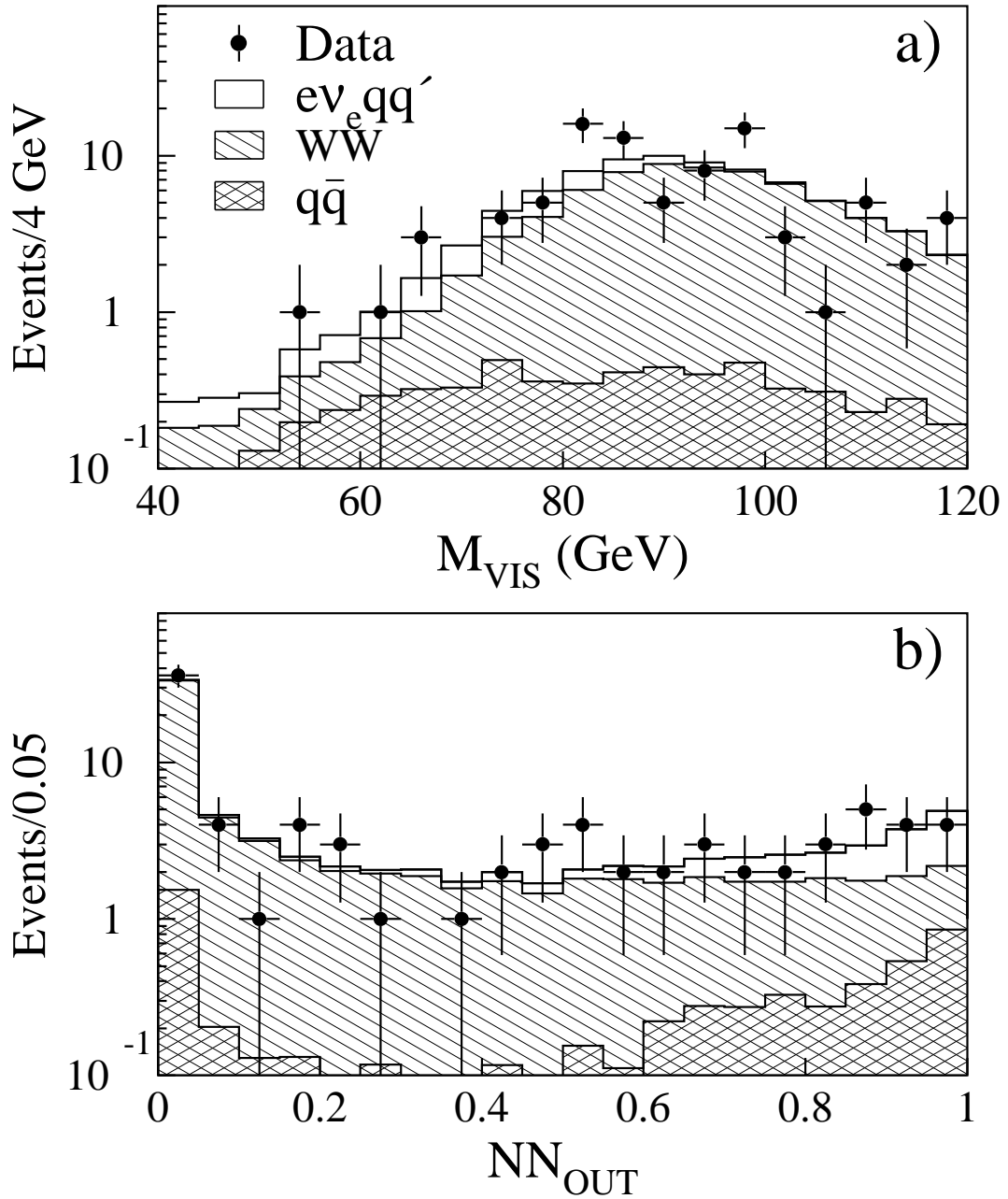


Figure 2: (a) The jet-jet invariant mass spectrum and (b) the neural network output distribution for the selected hadronic events at $\sqrt{s} = 183$ GeV. The dots are data, the hatched histograms represent the backgrounds and the open histograms show the expected signal from $e^+\nu_e q\bar{q}'$ final states.

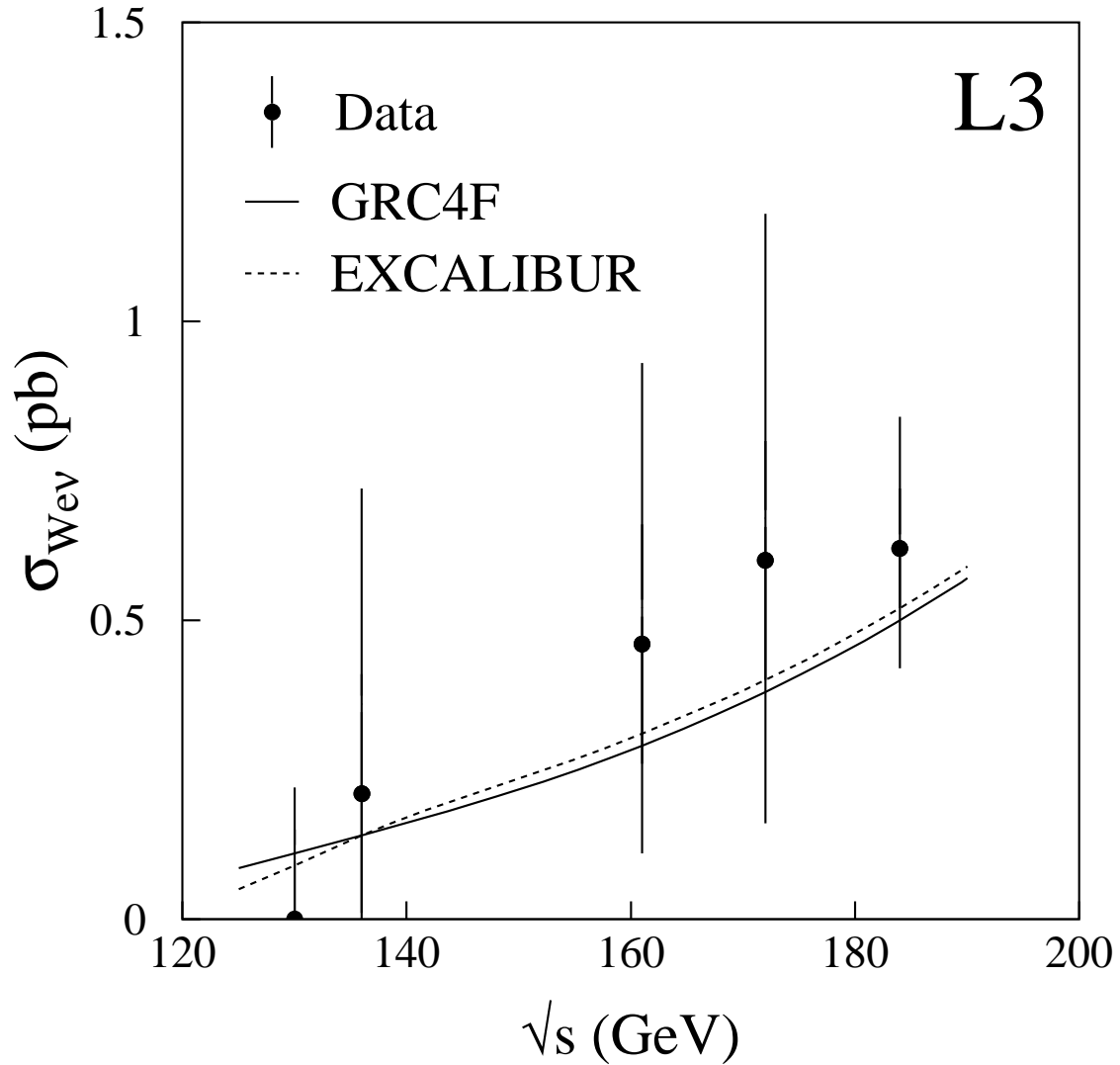


Figure 3: The measured cross section of single W production as a function of the centre-of-mass energy. Each point represents the most likely cross section value at a given centre-of-mass energy. The error bars correspond to the 68% confidence intervals obtained from the cross section fit. The solid and dashed lines show predictions of the GRC4F and EXCALIBUR Monte Carlo programs, respectively.

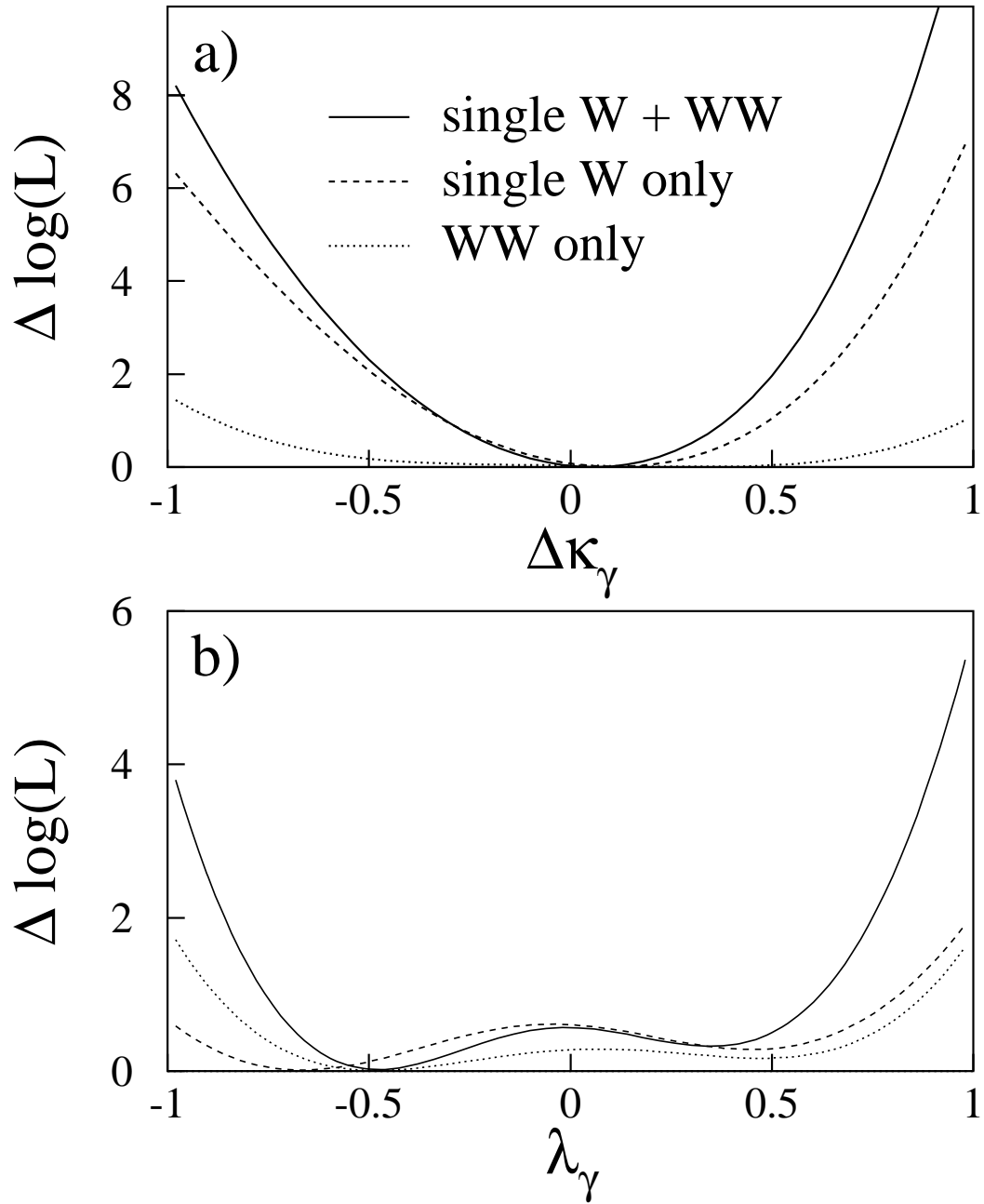


Figure 4: The dependence of the log-likelihood function, $\Delta \log(L)$, on the anomalous couplings (a) $\Delta \kappa_\gamma$ and (b) λ_γ in the vicinity of its minimum. For comparison, the individual contributions of the signal and the WW background are also shown.

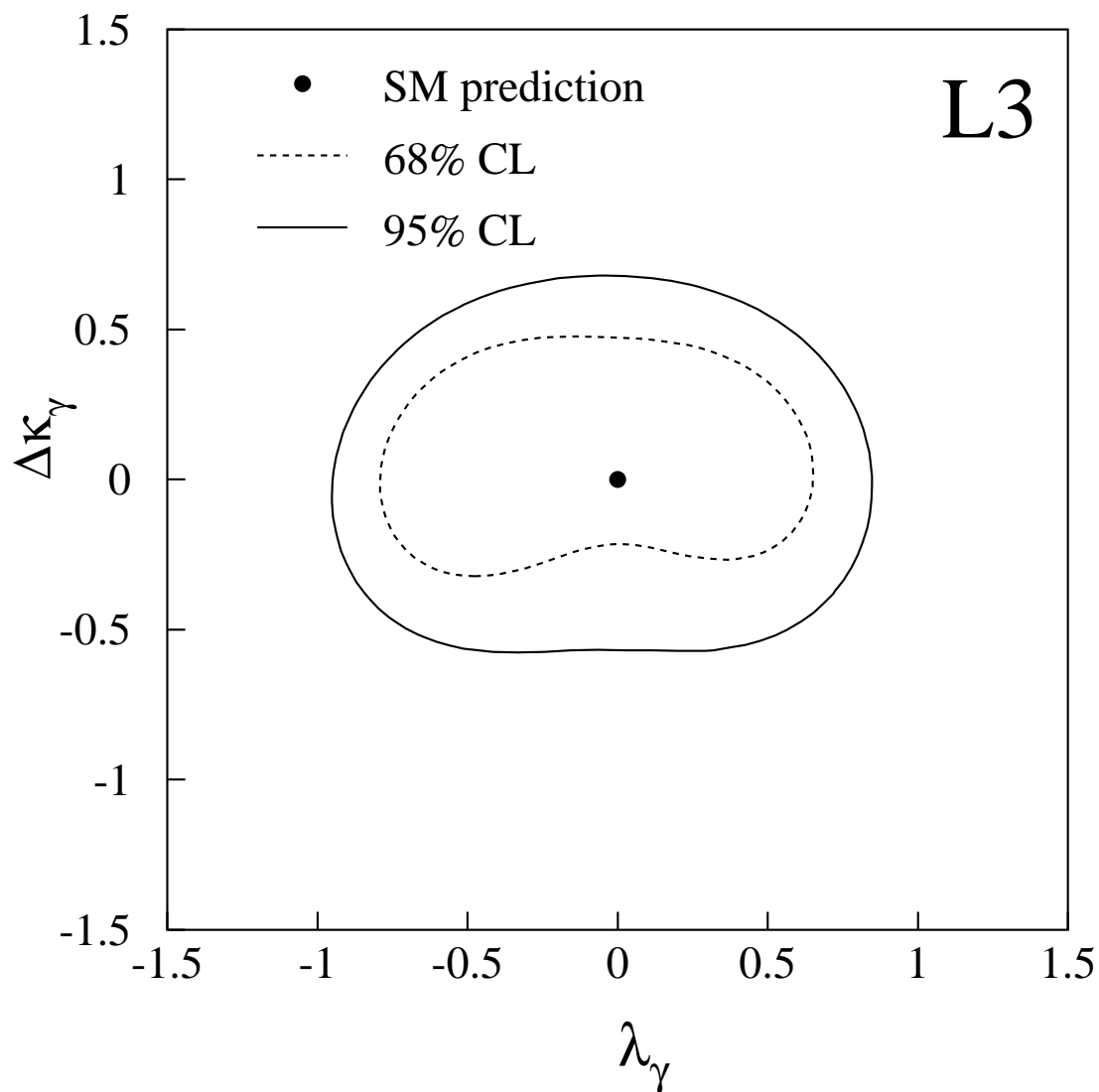


Figure 5: The contours corresponding to 68% and 95% confidence level in the $\Delta\kappa_\gamma - \lambda_\gamma$ plane.